SCIENCE CHINA
Technological Sciences

•Article•

February 2020 Vol.63 No.2: 214–222
https://doi.org/10.1007/s11431-018-9434-5

Effects of surface shapes on properties of turbulent/non-turbulent interface in turbulent boundary layers

WU Di, WANG JinJun*, CUI GuangYao & PAN Chong

Fluid Mechanics Key Laboratory of Education Ministry, Beijing University of Aeronautics and Astronautics, Beijing 100191, China

Received November 1, 2018; accepted January 4, 2019; published online June 6, 2019

The effects of directional riblets surfaces on the turbulent/non-turbulent (T/NT) interface in turbulent boundary layers are experimentally investigated using two-dimensional time-resolved particle image velocimetry (PIV). The velocity field of streamwise—wall-normal plane for the smooth surface, converging and diverging riblets surfaces are measured. The interface is detected using the criterion of local kinetic energy. The statistical properties of interface height and conditional averaged velocity for different surfaces are analyzed. It is shown that, the converging and diverging riblets surfaces have little effect on the fractal dimension of the T/NT interface, but they cause the intermittency profile deviate from error function and the probability distribution of interface height deviate from Gaussian function. To be specific, the distribution of interface height for the converging riblets surface shows a positive skewness while it shows a negative skewness for the diverging riblets surface. Moreover, the conditional averaged streamwise velocity and spanwise vorticity across the interface are analyzed, and it is found that their self-similarities are preserved for different surfaces when normalized with respective friction velocity. The correlation analysis reveals that near-wall streamwise velocity fluctuation and interface height show a negative correlation.

riblets surface, turbulent boundary layers, turbulent/non-turbulent (T/NT) interface, conditional averaging

Citation: Wu D, Wang J J, Cui G Y, et al. Effects of surface shapes on properties of turbulent/non-turbulent interface in turbulent boundary layers. Sci China Tech Sci, 2020, 63: 214–222, https://doi.org/10.1007/s11431-018-9434-5

1 Introduction

Turbulent/non-turbulent (T/NT) interface is the boundary between turbulent flow and irrotational flow. The T/NT interface exists in many kinds of flow fields such as turbulent patches in atmosphere, combustion flame front, impinging jets, turbulent wake, turbulent boundary layers, etc. The investigation of T/NT interface mainly focuses on the geometrical and dynamical properties.

The geometrical properties of the T/NT interface mainly contain intermittency profile, probability distribution of interface height, fractal-like properties of the interface, etc. Early work with hot-wire data, one cannot get the information of interface height from velocity signals of only several measurement points. They can only give the intermittency profile along the wall-normal direction through velocity fluctuation. Corrsin and Kisteler [1] pointed out that the cumulative distribution of interface height is equivalent to the intermittency distribution, such that one can take the derivative of intermittency to get the distribution of interface height from hot-wire signal. With the development of direct numerical simulations and flow field measurement technologies, it is possible to obtain the instant geometric shape of T/NT interface. Mistry et al. [2] obtained the distribution of T/NT interface position of an axisymmetric jet using particle image velocimetry (PIV) and planar laser-induced fluorescence (PLIF). They found that the radial position of T/NT interface at different streamwise location shows self-similarity when normalized by the local jet half-width. Similar to axisymmetric jet flow, the distribution of T/NT interface position in axisymmetric turbulent wake also shows self-similarity when normalized by wake width (Zhou and Vas-

*Corresponding author (email: jjwang@buaa.edu.cn)

silicos [3]). In the investigation of turbulent boundary layer, Borrell and Jiménez [4] pointed out that the distribution of interface height is related to the threshold chosen in interface detection. The mean position of interface decreases with the increase of threshold. Corrsin and Kistler [1] found that the thickness of intermittency zone is in the order of boundary-layer thickness, they also suggested that there is a viscous diffusion region and the thickness of which was estimated to be the order of Kolmogorov scale. The multiscale characteristic motivates the investigation of fractal-like properties of the T/NT interface (Sreenivasan et al. [5]). de Silva et al. [6] studied the fractal dimension of T/NT interface in turbulent boundary layer at high Reynolds numbers (Re_τ= 7900, 14500). They found that the fractal dimension is independent of Reynolds number. Besides, the threshold and the coarse graining process have little effect on fractal dimension.

The investigation on dynamical properties is based on the conditional averaged flow field across the interface. Corrsin and Kistler [1] proposed a hypothesis that there is a step change in velocity across the T/NT interface. In later work, the velocity jump is observed in wake flow, turbulent jet, turbulent boundary layer, etc. [7–9]. Corresponding to velocity jump there is a spanwise vorticity peak near the T/NT interface. Bisset et al. [7] investigated the far wake behind a thin flat plate using direct numerical simulations. They found that the velocity jump and spanwise vorticity peak appear around the interface within 0.1 of wake width. Westerweel et al. [10] found that the velocity jump in axisymmetric jet flow is about 9% of the center-line velocity. In the investigation of turbulent boundary layer, Chauhan et al. [11] found that the velocity jump with the value close to friction velocity appears at all Reynold number investigated.

There are many literatures investigating the T/NT interface at different Reynold numbers, but the effects of near-wall characteristics on the T/NT interface are not considered. Riblets surfaces, as a typical non-smooth wall, having ability to reduce the skin-friction drag, have received vast attention since 1980s [12–15]. Experimental (Bechert et al. [16]) and numerical (Martin and Bhushan [17]) studies have found that riblets surfaces can achieve skin friction reduction up to 10% with optimal normalized parameters (riblets spacing s^+=15 −20, height-to-spacing ratio h/s=0.5−0.7). There are two main explanations for drag reduction mechanism. The first explanation is that streamwise-aligned riblets reduce spanwise turbulent momentum transfer near the surface leading to a skin-friction reduction (Bechert et al. [16]). The other explanation is that when the spacing is appropriate, the riblets can achieve drag reduction by lifting the streamwise vortices away from the surface (Choi et al. [18]). Most of the literatures on riblets surfaces have been focused on the streamwise-aligned riblets. There are seldom literatures on other kind of arrangement (such as converging and diverging pattern (abbreviated as C-D pattern hereafter)). Koeltzsch et al. [19] investigated the effect of C-D riblets pattern in a fully developed turbulent pipe flow. The result shows that the tiny surface modification significantly influenced the mean velocity field. Nugroho et al. [20] investigated the C-D riblets pattern in turbulent boundary layer using hot-wire measurements. They found that converging and diverging riblets surfaces lead to a significant change in streamwise velocity, fluctuation intensity and boundary layer thickness. They also indicated that the riblets yaw angle, normalized riblets height and development length over the C-D riblets surfaces are the main parameters. Kevin et al. [21] investigated the velocity field in cross-stream plan using stereoscopic PIV and found that over the converging regions, there is a positive vertical flow, while over the diverging regions there is a negative vertical flow. The secondary flow induced by C-D riblets causes the differences in mean velocity and velocity fluctuation intensity, which will also affect the engulfment process. Cui et al. [22] investigated the population of prograde vortices and its contribution to the mean shear on converging and diverging riblets surfaces. They found that the diverging riblets surface reduces the population of prograde vortices which contribute significantly to the mean shear such that the diverging riblets surface can reduce the skin-friction drag. All these studies on both streamwise-aligned riblets and C-D riblets pattern surfaces have mainly focused on the friction velocity, flow structure near the wall, velocity and fluctuation intensity. But whether the near-wall characteristics will affect the properties of T/NT interface, the connection between skin-friction drag and the interface properties are not investigated.

The main purpose of present study is to reveal the effects of riblets surfaces on the properties of T/NT interface. The structure of this paper is organized as follows: The experimental setups and the geometry parameters of the models are introduced in Sect. 2. The basic flow fields of smooth surface, converging and diverging riblets surfaces are briefly presented in Sect. 3.1. Sect. 3.2 introduces the interface detection method used in this investigation and the overall characteristics of the T/NT interface. Sects. 3.3 and 3.4 compare the differences in statistical properties and conditional averaged velocity field among smooth surface, converging and diverging riblets surfaces. Sect. 3.5 analyzes the correlation between near wall streamwise velocity fluctuation and interface height. A summary of main conclusions is presented in Sect. 4.

2 Experimental setups

Experiments were conducted in a low-speed recirculation water channel with a test section of 700 mm×600 mm×3000 mm (height×width×length). The free-stream velocity was set

at U_∞=194 mm s^{-1}, with the corresponding free-stream turbulence intensity Tu≤0.6%. The three models are smooth surface, converging and diverging riblets surfaces flat plates. The size of models is 20 mm×600 mm×2400 mm (thickness×width×length). The flat plate with a 10:1 slant leading edge was horizontally positioned on the bottom of the water channel. A tripping wire with the diameter of 3 mm was used to accelerate transition. The measurement station was 1850 mm downstream the tripping wire. The measurement plane was 300 mm from the sidewall of the channel, far enough to be free from the effect of sidewall whose boundary layer thickness is less than 30 mm. A schematic of converging riblets surface flat plate is given in Figure 1(a). A definition of several important parameters is also given in Figure 1(a). The riblets yaw angle is defined as the angle between extension cord of the riblets on the right side and the flow direction. The riblets yaw angle of converging riblets surface is α=15°, while the diverging riblets surface is α=−15°. A detailed view of the riblets cross-section is given in Figure 1(b). The riblets spacing s=1.932 mm, height h=1.5 mm and tip angle β=60° are fixed for both converging and diverging riblets surfaces. A 0.2 mm flat exists in the riblets trough due to chamfered tip of the CNC cutter. The aim of our study is to investigate the effects of converging and diverging riblets surfaces on properties of T/NT interface. The small flat has not much influence on our investigation here. In the following, the streamwise, wall-normal, and spanwise are represented by x, y, z respectively, and u, v and w represent the corresponding velocity component. The subscript "c" donates quantities of the conditional average. The subscript "i" donates quantities at the interface.

The flow field in the middle plane of side view (x, y) was measured by the 2-D time-resolved PIV system. The flow field was illuminated by a high-frequency double-pulsed laser (Beamtech Vlite-Hi-30k) with output energy of 30 mJ/pulse and highest frequency of 3 kHz. The tracing particles were hollow glass beads with median diameter of 10 μm and density of 1.05 g cm^{-3}. A high-speed CMOS camera with a spatial resolution of 2048×2048 pixels in together with a 90 mm lens were used to capture the particle images. The sampling frequency in the experiments was 500 Hz. The field of view (FOV) was 98 mm×98 mm (2.1δ×2.1δ for smooth surface boundary layer) corresponding to the magnification of 0.045 mm pix^{-1}. For each case, 5 repetitions of continuous PIV sampling were made with 5456 frames captured each time. Corresponding to a total ensemble of more than 27000 snapshots for each case, large enough for the convergence of statistics. The multi-pass iterative Lucas-Kanade (MILK) algorithm (Champagnat et al. [23]; Pan et al. [24]) was applied to calculate the velocity vector fields. The interrogation window for the final pass was 32 pixel×32 pixel with an overlap of 75%.

3 Results and analysis

3.1 Velocity measurements

The details of experimental cases and basic flow fields can be found in Cui et al. [22]. We will only briefly discuss here. For the smooth flat plate, the friction velocity can be obtained with Clauser fitting method. For the converging and diverging riblets surfaces, owing to the offset of origin, the Clauser fit method cannot be used directly. Nugroho et al. [20] used a modified Clauser technique to estimate friction velocity.

$$u^+ = \frac{1}{\kappa}\ln\hat{y}^+ + B - \Delta u^+, \tag{1}$$

where $\hat{y}$ is defined as the wall-normal distance from the crest of riblets (y) plus the offset due to roughness (y_v), Δu^+ is a positive number for drag increasing surfaces, and a negative number for drag reduction surfaces. By performing differential on both sides of eq. (1) we can get

$$\frac{\Delta u}{\Delta y} = \frac{u_\tau}{\kappa}\frac{1}{y+y_v}. \tag{2}$$

The offset due to roughness (y_v) and friction velocity (u_τ) of converging and diverging riblets surfaces fitted by eq. (2) are presented in Figure 2. The characteristic boundary layer parameters are listed in Table 1. The velocity field of smooth surface shows good agreement with Clauser fit which means the flow in the FOV is fully turbulent. For converging riblets

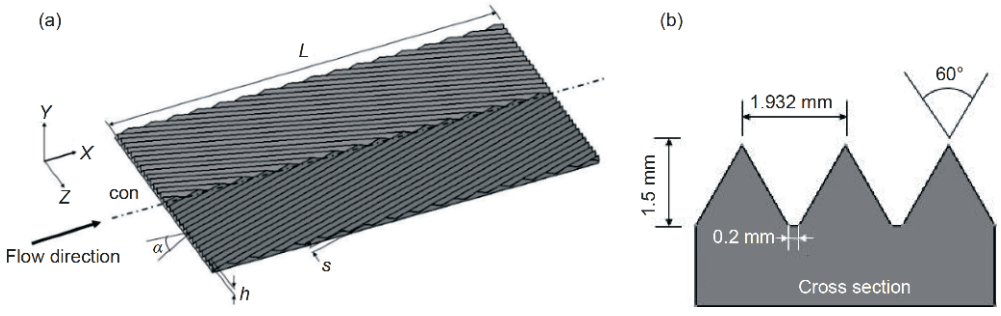

Figure 1 Sketch of experimental model and definition of the coordinates (Cui et al. [22]). (a) Schematic drawing of the converging riblets surface flat plate; (b) sketch of riblets cross-section. The riblets in (a) are enlarged in scale for clarity.

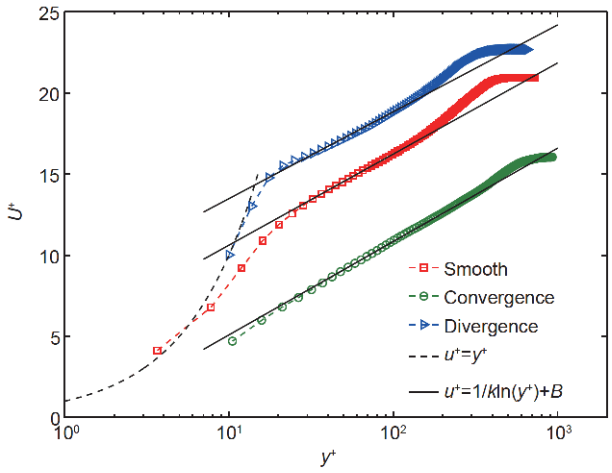

Figure 2 (Color online) Profiles of the ensemble-averaged streamwise velocity (Cui et al. [22]). Symbols show the smooth surface (□); converging riblets surface (○); diverging riblets surface (▷). Solid lines give the Clauser fit.

surface, Δu^+ is positive (Δu^+= 5.67) and the friction velocity u_τ is bigger than smooth surface. Meanwhile, the turbulent boundary layer thickness is increased. As for diverging riblets surface, the roughness function Δu^+ is negtive (Δu^+= –3.03) and the friction velocity u_τ is smaller than smooth surface. For the diverging riblets surface, the turbulent boundary layer thickness is reduced. The difference in roughness function suggests that the wall drag is increased over converging riblets surface and decreased over diverging riblets surface.

3.2 Detection of T/NT interface

The T/NT interface is detected using a kinetic energy (KE) criterion proposed by Chauhan et al. [25]. The local kinetic energy is defined as

$$\tilde{k} = 100 \times \frac{1}{9U_\infty^2} \sum_{m,n=-1}^{1} \left[(\tilde{U}_{m,n} - U_\infty)^2 + (\tilde{V}_{m,n})^2 \right]. \quad (3)$$

Above the interface, in the non-turbulent region, $\tilde{k}$ would be a very small value. Below which, $\tilde{k}$ would increase with the normal distance from the interface. Such that $\tilde{k}$ forms a good indicator in the detection of T/NT interface. The determination of threshold k_{th} has also been given by Chauhan et al. [25]. The threshold should meet both conditions: the distribution of intermittency agrees with an error function, the mean position of interface (Y_{i}) and standard deviation (σ_{i}) satisfy $Y_{\text{i}}+3\sigma_{\text{i}}\approx\delta$ (δ is the boundary layer thickness). In our experiments, the threshold of smooth surface was set to be k_{th}=0.2. For the converging and diverging riblets surfaces, we cannot find a threshold k_{th} which can meet both conditions. Since the free-stream turbulence intensity and velocity field calculation algorithm of riblets surfaces are the same with smooth surface. The threshold of smooth surface with the same free-stream velocity was used.

An example of instantaneous interface over smooth surface is given in Figure 3. The background contours represent the instantaneous streamwise velocity in company with the T/NT interface gives in black lines. The T/NT interface of a three-dimensional turbulent boundary layer should be a two-dimensional surface. The interface we detected from the two-dimensional velocity field is the intersecting line of the two-dimensional surface and the streamwise—wall-normal plane. In our FOV, the interface height varies significantly along the streamwise direction, forms bugles and valleys. Meanwhile, there are small-scale wrinkles at the interface. These large-scale and small-scale structures lead to multiple interface height at several streamwise locations. The interface convects downstream, meanwhile the interaction between the potential flow and turbulent flow at the interface will result in deformation of the interface.

3.3 Detection of T/NT interface

In the FOV, the small riblets ($h/\delta\approx$0.03) have caused a significant difference in boundary layer thickness and near wall flow structure. Such as the boundary layer thickness of converging riblets surfaces is thickened by 40% and the friction velocity is enlarged (Table 1). In this section, the effect of riblets surfaces on statistical properties of T/NT interface will be studied.

The instantaneous T/NT interface height can be caught by evaluating the isoline of local kinetic energy $\tilde{k} = k_{\text{th}}$. Since the streamwise distance is small (about 2δ) and the turbulent boundary layer is fully developed, the mean velocity profile can be assumed the same in our FOV. For better statistical convergence, the interface height at different streamwise locations are all considered. The probability density function (p.d.f.) of interface height for smooth surface, converging and diverging riblets surfaces are shown in Figure 4. For smooth surface, except for the deviation of very few points, the p.d.f. agrees well with Gaussian function. The mean interface height is Y_{i}=0.67δ and the standard deviation is σ_{i} =0.13δ. The T/NT interface of smooth surface located in the

Table 1 Summary of the characteristic boundary layer parameters (Cui et al. 2017)

Case	U_∞ (mm/s)	α	u_τ (mm/s)	δ (mm)	s^+	h^+	Re_τ	Re_θ
Smooth	194.3	0	9.3	46.3	–	–	483	892
Convergence	194.6	15°	12.2	66.1	26.3	20.4	903	1242
Divergence	194.2	–15°	8.6	45.4	18.5	14.4	422	739

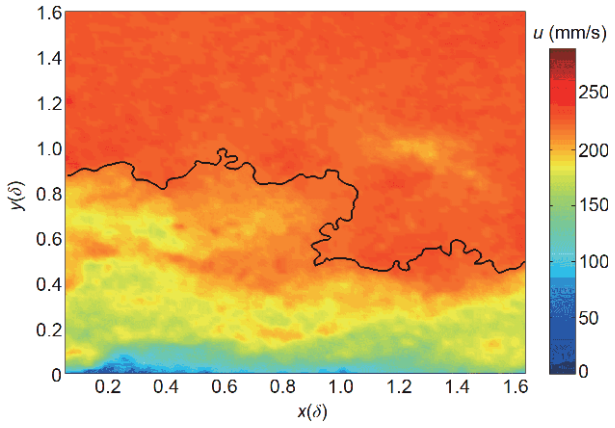

Figure 3 Streamwise velocity field (background contours) in comparison with T/NT interface (black lines).

range of 0.3–1.0δ (corresponding to 0.37–1.27δ_{99}). The mean interface height and standard deviation agree well with previous data listed in Table 2. For better comparison, the normalization with δ and δ_{99} are both given. The Reynolds number in present experiment is smaller than previous work (as seen in Table 2). The agreement expands the range in which the distribution of interface height is independent of Reynold number. For converging riblets surface, the mean interface height is Y_i=0.63δ (Figure 4(b)), much smaller than smooth surface; meanwhile the standard deviation is σ_i=0.14δ (Figure 4(b)), slightly larger than smooth surface. More importantly, the distribution of interface height for converging riblets surface deviates from Gaussian function, it shows a significant positive skewness of Skew$_i$=0.66, which makes the peak of p.d.f smaller than the mean interface height. As for diverging riblets surface, the mean interface height is Y_i=0.58δ, also much smaller than smooth surface, while the standard deviation is similar (σ_i=0.13δ). The distribution deviates from Gaussian function as well and shows a slight negative skewness of Skew$_i$=−0.10, which makes the peak of p.d.f slightly larger than the mean interface height. The mean common flow up over converging riblets surface (Kevin et al. [21]) will lift the instantaneous interface, result in the positive long tail in distribution of interface height. While the mean common flow down over diverging riblets surface will diminish the interface, results in a negative skewness.

The method to get the turbulent and non-turbulent region has been introduced in Sect. 2.2. Binarizing the velocity matrix by assigning the turbulent region to be 1, and the non-turbulent region to be 0. The intermittency profile can be calculated by taking ensemble average of the binarized matrix at different wall-normal position. It is shown in Figure 5 that the intermittency profile of smooth surface does agree well with error function, which confirms the statistical properties we got before. As for converging and diverging riblets surfaces, the intermittency profiles deviate from error function, which are in accordance with deviation from Gaussian function of interface height. The physical wall-normal height for the converging riblets surface with intermittency γ=0.5 is larger than smooth surface, while which is smaller for the diverging riblets surface. However, when normalized with respective boundary layer thickness, wall-normal positions with γ=0.5 of both converging and diverging riblets surfaces are smaller than smooth surface, which are caused by the significantly thickened boundary layer

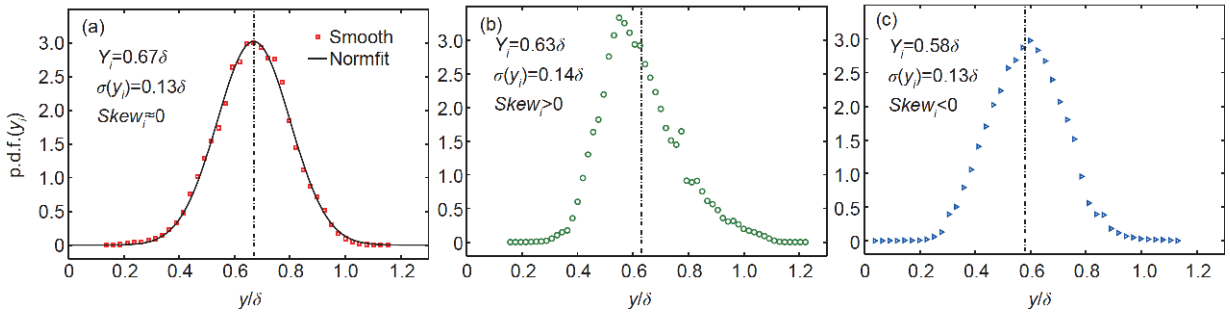

Figure 4 The probability density function of interface height. Symbols show the (a) smooth surface (□); (b) converging riblets surface (○); (c) diverging riblets surface (▷). Dashed line represents the mean interface height.

Table 2 Comparison of mean interface height and standard deviation

Case	Re_τ	Y_i/δ	σ_i/δ	Y_i/δ_{99}	σ_i/δ_{99}
Corrsin and Kistler [1]	<2000	–	–	0.80	0.16
Eisma et al. [26]	2053	–	–	0.90	0.18
Chauhan et al. [10]	2700-22000	0.67	0.11-0.13	–	–
Chauhan et al. [25]	14500	0.67	0.11	–	–
Present work (smooth)	483	0.67	0.13	0.82	0.16

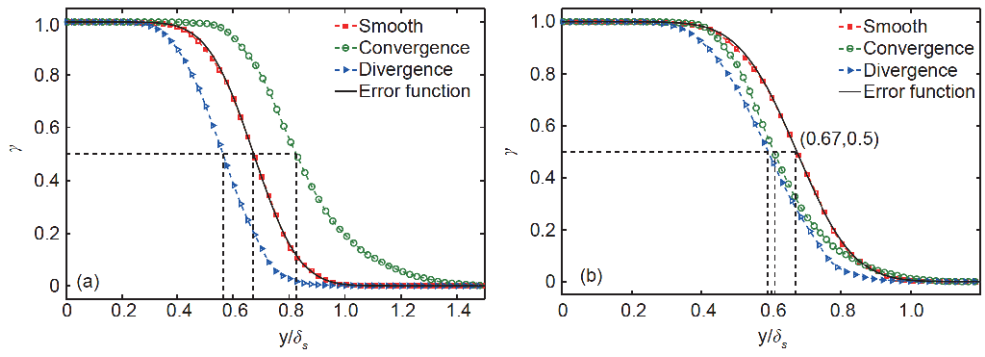

Figure 5 (Color online) Intermittency profile. (a) Normalized by smooth surface boundary layer thickness; (b) normalized by respective boundary layer thickness. Symbols show the smooth surface (□); converging riblets surface (○); diverging riblets surface (▷). Solid lines give the error function. Dashed lines give γ=0.5 and the corresponding height.

thickness for the converging riblets surface and slightly thinned for the diverging riblets surface. It should be noted that since the intermittency profiles deviate from error function, the position with γ=0.5 is no longer the mean position of interface height, it only represents the wall-normal position of flow with equal possibility at turbulent and non-turbulent state.

The fractal characteristics in turbulence were first suggested by Mandelbrot [27] who pointed out that the turbulent eddies may have fractal characteristic at high Reynolds number. Sreenivasan et al. [28] was the first one who found fractal characteristics in T/NT interface. The fractal dimension is related to the complexity of the interface. The entrainment per unit area is similar in all turbulent flows (Townsend [29]), fractal dimension will represent the entrainment rate in different turbulent flow. The box-counting algorism proposed by Prasad and Sreenivasan [30] is used here to calculate the fractal dimension of T/NT interface: divide the two-dimensional field into square boxes of a certain size (b/δ), the minimum number of boxes $N(b)$ needed to contain all the instantaneous interface is recorded. The process is repeated at each frame for a sequence of box size. In an appropriate range, the average value of box size b/δ and box number N will satisfy $N\propto(b/\delta)^{-D}$, in which D is the fractal dimension. When plotted in log-log coordinate, b/δ and N will be linear-like and the slop will be fractal dimension D. Figure 6 shows the fractal dimensions of smooth surface, converging and diverging riblets surfaces. The range we used for linear fit is given in Figure 6 by dashed lines. For all three surfaces, the fractal dimension kept the same at D = −1.22 corresponding to D_f = 2.22 in three-dimension according to the co-dimension rule proposed by Mandelbrot et al. [31]. de Silva et al. [6] experimentally obtain the fractal dimension D_f =2.3 in turbulent boundary layer at Reynold number Re_τ=14500. The fractal dimension obtained here is relatively smaller, which may be owing to the low Reynolds number here. The large scale and small scale is not sufficiently separated.

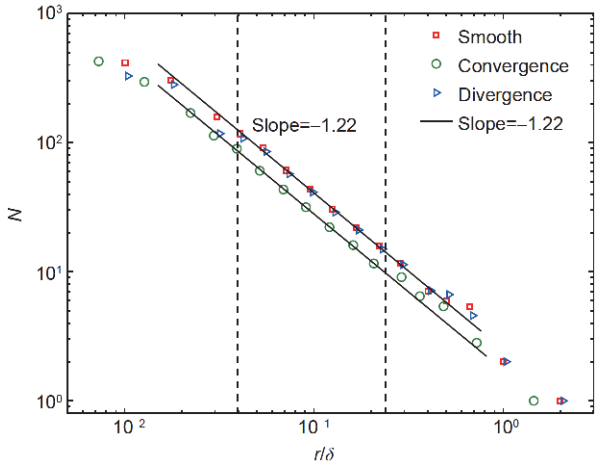

Figure 6 (Color online) The fractal dimension of different surfaces. Symbols show the smooth surface (□); converging riblets surface (○); diverging riblets surface (▷). Dashed lines represent the range used for linear fit.

3.4 Conditional averaged velocity

The statistical properties of interface height have been analyzed in Sect. 2.3. The change of distribution of interface height will influence the flow field near the interface. In this section, the conditional averaged velocity profiles of different surfaces are analyzed. For every streamwise position at each frame, new coordinates are built by putting the origin at interface position, while the coordinate direction is kept the same. The velocity vectors in the vicinity of interface can be collected in a new matrix. Then an ensemble average is made to generate the conditional averaged velocity fields. As seen in Figure 3, at some streamwise position the interface has multiple values. Only the lowest one is considered to make sure that the flow is fully turbulent below the interface (Chauhan et al. [25]).

Figure 7 shows the conditional averaged streamwise velocity profiles of different surfaces. Above the interface in

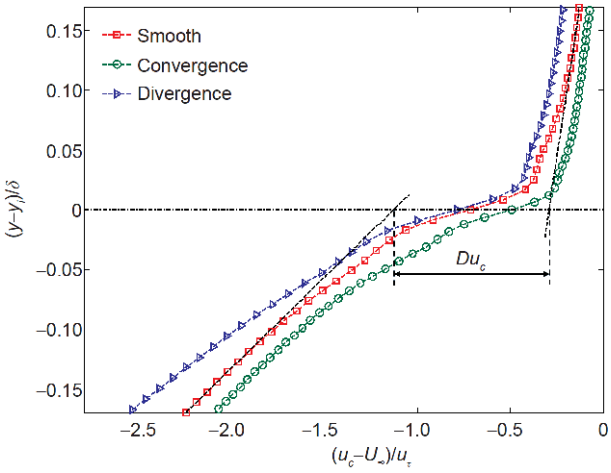

Figure 7 (Color online) Conditional averaged streamwise velocity with respect to the wall-normal distance from the interface. Symbols show the smooth surface (□); converging riblets surface (○); diverging riblets surface (▷). Dot dash line represents the new x-coordinate. Dashed lines represent the linear fit of conditional velocity profile on both sides of the interface.

the non-turbulent region, the velocity gradient is very small, while below the interface in the turbulent region, the velocity gradient is relatively larger. A velocity jump appears in the vicinity of the interface for all three profiles, which correspond to a peak in velocity gradient. Chauhan et al. [11] have shown the conditional averaged velocity profiles at different Reynolds numbers. The conditional mean streamwise velocity at the interface is similar to each other, while the difference exists in the region of $-0.01 \le (y-y_i)/\delta \le 0.05$. The riblets surfaces, however, caused the difference in streamwise velocity in the whole wall-normal position around the interface. We calculated the velocity jump of all three surfaces using the method proposed by Chauhan et al. [25]: the distance between intersection points, formed by the new x-coordinate with linear fit of conditional velocity profiles on both sides (Du_c shown in Figure 7). The velocity jump of smooth surface, converging and diverging riblets surfaces

Table 3 Comparison of velocity jump and vorticity peak

Case	Du_c/U_∞	Du_c/u_τ	δ_ω/δ	$(du_c/dy)_{max}\,\delta/U_\infty$	$(du_c/dy)_{max}\,\delta/u_\tau$
Smooth	4.0%	0.83	0.034	1.16	24.2
Convergence	5.0%	0.80	0.033	1.49	23.9
Divergence	3.5%	0.80	0.033	1.08	24.5

are listed in Table 3. Even though the conditional averaged velocity profile is different, the velocity jump keeps the same when normalized by respective friction velocity. Whereas if normalized by free-stream velocity, the velocity jump for the converging riblets surface is larger than smooth surface, while for the diverging riblets surface is smaller.

The thickness where the velocity jump occurs can be defined as

$$\delta_\omega = \frac{Du_c}{(du_c/dy)_{max}}, \tag{4}$$

where Du_c is the velocity jump, $(du_c/dy)_{max}$ is the maximum velocity gradient. The velocity jump occurs in turbulent sublayer, which is much thicker than viscous superlayer (Watanabe et al. [32]). So the thickness defined above can be regarded as an approximate thickness of T/NT interface. The interface thickness is independent of near-wall characteristics (as seen in Table 3).

The conditional averaged spanwise vorticity is plotted in Figure 8. Dashed lines represent the T/NT interface region. Above the interface, the spanwise vorticity is close to zero, which means the flow is basically irrotational. Below the interface, the spanwise vorticity is approximately a finite number. In the region of δ_ω, the spanwise vorticity reaches a peak. The maximum value of spanwise vorticity is listed in Table 3. When normalized with U_∞/δ, the spanwise vorticity shows great difference. For the converging riblets surface, the maximum value is much larger than smooth surface, while for the diverging riblets surface is smaller. The difference in spanwise vorticity peak is in accordance with the

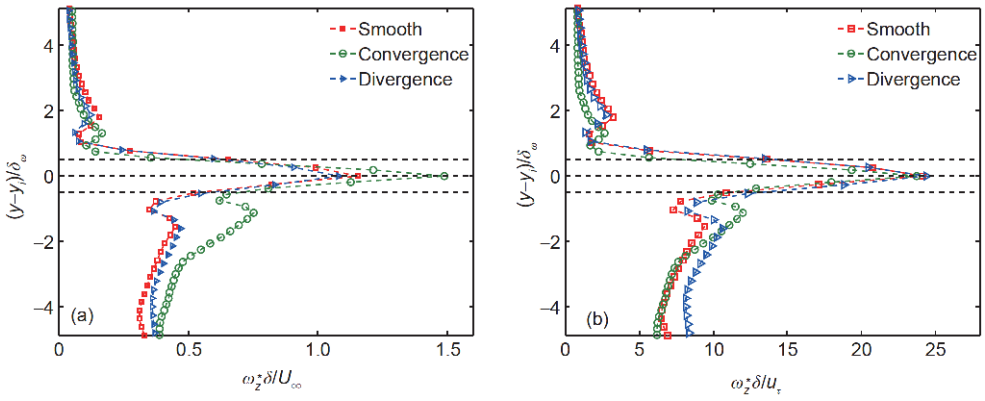

Figure 8 (Color online) Conditional averaged spanwise vorticity with respect to the wall-normal distance from the interface. Symbols show the smooth surface (□); converging riblets surface (○); diverging riblets surface (▷). The dashed lines represent the thickness of interface. (a) Spanwise vorticity normalized with U_∞/δ; (b) spanwise vorticity normalized with u_τ/δ.

velocity jump for different surfaces. Whereas, if normalized with u_τ/δ, the value agrees well with each other for different surfaces (Figure 8(b)).

The consistency in velocity jump and vorticity peak normalized with friction velocity for three surfaces inspired us that the fiction velocity can be estimated by a new method: The accurate estimate of friction velocity on riblets surfaces is difficult for two reasons. The uncertainty of origin and the wall reflection caused by riblets. For smooth surface, with more satisfied velocity models and slighter wall reflection, the friction velocity can be estimated much better. Such that the friction velocity for converging and diverging riblets surfaces can be calculated based on the consistency in velocity jump and vorticity peak with smooth surface at the same free-stream velocity. Friction velocity estimated with data in intermittency region is free from wall reflection and other near wall errors. The present experiments for different surfaces were conducted at a single free-stream velocity, the results are welcomed to be confirmed with more data at different free-stream velocities.

3.5 Correlation analysis

Near wall streamwise velocity fluctuation intensity and flow structures are significantly changed over converging and diverging riblets surfaces (Cui et al. [22]). A correlation analysis between interface height and velocity fluctuation (at inner peak of streamwise velocity fluctuation intensity) is conducted to reveal the mechanism of the effect of surface shapes on properties of T/NT interface. The interface height signal and streamwise velocity fluctuation signal at wall-normal position $y^+\approx15$ (inner peak) over smooth surface are shown in Figure 9. The original signals are divided into large-scale and small-scale components by an FFT based on decomposition method with a cutoff length scale $\lambda_x=\delta$. It can be seen from Figure 9 that the large-scale components of streamwise velocity fluctuation and interface height shows a negative correlation, while the small-scale components seems to be irrelevant to each other. It should be noted that to make both signals distinct, the large-scale and small-scale components of streamwise velocity fluctuation are moved to the $-y$ direction with Δy=0.4. To further illustrate the correlation, the correlation coefficient between large-scale/small-scale components of streamwise velocity fluctuation and interface height ($Ru_L y_{iL}$, $Ru_S y_{iS}$) at different cutoff wavelength are calculated. In Figure 10, the horizontal axis is the cutoff length scale, while the vertical coordinate is the correlation coefficient at this wavelength. Since the correlation coefficient between large-scale/small-scale component of streamwise velocity fluctuation and small-scale/large-scale component of interface height ($Ru_L y_{iS}$, $Ru_S y_{iL}$) is close to 0 for all cutoff length scales, they were not shown in

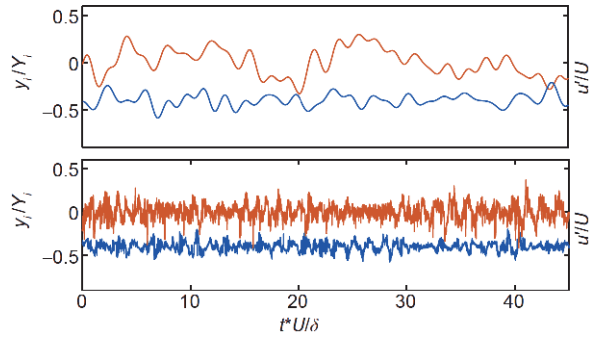

Figure 9 Near wall streamwise velocity fluctuation intensity signal (red line) and interface height signal (blue line). The interface signal is normalized with mean interface height Y_i, streamwise velocity fluctuation is normalized with free-stream velocity U_∞. (a) Large-scale components; (b) small-scale components.

Figure 10. When the cutoff wavelength is located between 0.02δ−1δ, the correlation coefficient of small-scale component $Ru_S y_{iS}$ is close to 0, which indicates that the small-scale components are random fluctuation of velocity and interface height. The large-scale components of streamwise velocity fluctuation and interface height show a significant negative correlation with coefficient $Ru_L y_{iL} \approx -0.2$, which indicates that the interface is above the mean position when negative near wall velocity fluctuation occurs, while the interface is below the mean position when positive near wall velocity fluctuation occurs. The correlation analysis between interface height and velocity fluctuation at inner peak over converging and diverging riblets surfaces are also conducted. The correlation coefficients of large scale components are similar to smooth surface, which are also negative with the value close to $Ru_L y_{iL} \approx -0.2$. The negative correlation illustrates that the surface shapes not only affect the near wall flow, but exist up to the edge of turbulent boundary layers.

4 Conclusions

The properties of T/NT interface over smooth surface, con-

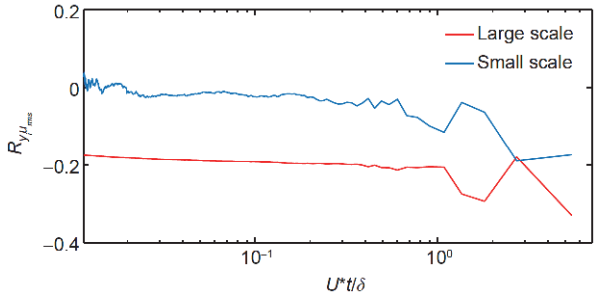

Figure 10 Correlation coefficient between large-scale/small-scale components of near wall streamwise velocity fluctuation and interface height of smooth surface. Red line represents coefficient $Ru_L y_{iL}$, blue line represents coefficient $Ru_S y_{iS}$.

verging and diverging riblets surfaces were calculated with 2-D time-resolved PIV data. The effects of surface shapes on statistical properties and conditional averaged velocity were analyzed. The main conclusions are as follows.

(1) The surface shapes show a significant effect on the statistical properties of the T/NT interface. The distributions of interface height deviate from Gaussian function for converging and diverging riblets surfaces. The mean interface height is smaller than that of smooth surface for converging riblets surface with a significant positive skewness, while it is smaller with a slight negative skewness for diverging riblets surface. Despite the significant difference in large-scale characteristic wavelength the near-wall characteristics show little influence on the fractal dimension of T/NT interface.

(2) Velocity jump and vorticity peak are observed near the interface for all three surfaces. When normalized with respective friction velocity, the velocity jump and vorticity peak are in consistent with each other, which indicates a new method to estimate the friction velocity on riblets surfaces.

(3) Near-wall streamwise velocity fluctuation and interface height show a negative correlation. The interface is above the mean position when negative near wall velocity fluctuation occurs, while the interface is below the mean position when positive near wall velocity fluctuation occurs. The influence of surface shapes extends to the edge of turbulent boundary layers.

This work was supported by the National Natural Science Foundation of China (Grant Nos. 91852206, 11721202, 11490552).

1 Corrsin S , Kistler A L . Free-Stream Boundaries of Turbulent Flows. Technical Report. Archive & Image Library, 1954
2 Mistry D, Philip J, Dawson J R, et al. Entrainment at multi-scales across the turbulent/non-turbulent interface in an axisymmetric jet. J Fluid Mech, 2016, 802: 690–725
3 Zhou Y, Vassilicos J C. Related self-similar statistics of the turbulent/non-turbulent interface and the turbulence dissipation. J Fluid Mech, 2017, 821: 440–457
4 Borrell G, Jiménez J. Properties of the turbulent/non-turbulent interface in boundary layers. J Fluid Mech, 2016, 801: 554–596
5 Sreenivasan K R, Meneveau C. The fractal facets of turbulence. J Fluid Mech, 1986, 173: 357–386
6 de Silva C M, Philip J, Chauhan K, et al. Multiscale geometry and scaling of the turbulent-nonturbulent interface in high Reynolds number boundary layers. Phys Rev Lett, 2013, 111: 044501
7 Bisset D K, Hunt J C R, Rogers M M. The turbulent/non-turbulent interface bounding a far wake. J Fluid Mech, 2002, 451: 383–410
8 Watanabe T, Sakai Y, Nagata K, et al. Turbulent mixing of passive scalar near turbulent and non-turbulent interface in mixing layers. Phys Fluids, 2015, 27: 085109
9 Jiménez J, Hoyas S, Simens M P, et al. Turbulent boundary layers and channels at moderate Reynolds numbers. J Fluid Mech, 2010, 657: 335–360
10 Westerweel J, Fukushima C, Pedersen J M, et al. Mechanics of the turbulent-nonturbulent interface of a jet. Phys Rev Lett, 2005, 95: 174501
11 Chauhan K, Philip J, Marusic I. Scaling of the turbulent/non-turbulent interface in boundary layers. J Fluid Mech, 2014, 751: 298–328
12 Walsh M J. Riblets as a viscous drag reduction technique. AIAA J, 1983, 21: 485–486
13 Choi K S. Near-wall structure of a turbulent boundary layer with riblets. J Fluid Mech, 1989, 208: 417–458
14 Wang J J, Lan S L, Miao F Y. Drag-reduction characteristics of turbulent boundary layer flow over riblets surfaces (in Chinese). Shipbuild China, 2001, 42: 1–5
15 Garcíamayoral R, Jiménez J. Drag reduction by riblets. Phil Trans R Soc A, 2011, 369: 1412–1427
16 Bechert D W, Bruse M, Hage W, et al. Experiments on drag-reducing surfaces and their optimization with an adjustable geometry. J Fluid Mech, 1997, 338: 59–87
17 Martin S, Bhushan B. Fluid flow analysis of a shark-inspired microstructure. J Fluid Mech, 2014, 756: 5–29
18 Choi H, Moin P, Kim J. Direct numerical simulation of turbulent flow over riblets. J Fluid Mech, 1993, 255: 503–539
19 Koeltzsch K, Dinkelacker A, Grundmann R. Flow over convergent and divergent wall riblets. Exp Fluids, 2002, 33: 346–350
20 Nugroho B, Hutchins N, Monty J P. Large-scale spanwise periodicity in a turbulent boundary layer induced by highly ordered and directional surface roughness. Int J Heat Fluid Flow, 2013, 41: 90–102
21 Kevin K, Monty J P, Bai H L, et al. Cross-stream stereoscopic particle image velocimetry of a modified turbulent boundary layer over directional surface pattern. J Fluid Mech, 2017, 813: 412–435
22 Cui G Y, Pan C, Gao Q, et al. Flow structure in the turbulent boundary layer over directional riblets surfaces (in Chinese). Chin J Theor Appl Mech, 2017, 49: 1201–1212
23 Champagnat F, Plyer A, Le Besnerais G, et al. Fast and accurate PIV computation using highly parallel iterative correlation maximization. Exp Fluids, 2011, 50: 1169–1182
24 Pan C, Xue D, Xu Y, et al. Evaluating the accuracy performance of lucas-kanade algorithm in the circumstance of piv application. Sci China-Phys Mech Astron, 2015, 58: 104704
25 Chauhan K, Philip J, de Silva C M, et al. The turbulent/non-turbulent interface and entrainment in a boundary layer. J Fluid Mech, 2014, 742: 1–33
26 Eisma J, Westerweel J, Ooms G, et al. Interfaces and internal layers in a turbulent boundary layer. Phys Fluids, 2015, 27: 055103
27 Mandelbrot B B. On the geometry of homogeneous turbulence, with stress on the fractal dimension of the iso-surfaces of scalars. J Fluid Mech, 1975, 72: 401–416
28 Sreenivasan K R, Ramshankar R, Meneveau C. Mixing, entrainment and fractal dimensions of surfaces in turbulent flows. Proc R Soc A-Math Phys Eng Sci, 1989, 421: 79–108
29 Townsend A A. The Structure of Turbulent Shear Flow. Cambridge: Cambridge University Press, 1976
30 Prasad R R, Sreenivasan K R. Scalar interfaces in digital images of turbulent flows. Exp Fluids, 1989, 7: 259–264
31 Mandelbrot B B, Wheeler J A. The Fractal Geometry of Nature. New York: Springer, 1983
32 Watanabe T, da Silva C B, Sakai Y, et al. Lagrangian properties of the entrainment across turbulent/non-turbulent interface layers. Phys Fluids, 2016, 28: 135–338